

1320 Beal Avenue
Ann Arbor, MI 48109-2140
(630) 200-3702
April 26, 2019

Philip Wdowiak, Team Captain
M-Fly Student Design Team
2603 Draper Dr
Ann Arbor, MI, 48109

Subject: Final report transmittal for structural testing and preliminary analysis of aluminum and carbon fiber landing gear

Dear Mr. Wdowiak:

Enclosed is our final report for the structural testing and analysis of aluminum and composite landing gear for use in future designs for M-Fly.

This report includes our results from testing the aluminum landing gear used on the MX-3, as well as an in-house carbon fiber layup that was conducted at the University of Michigan. As you requested, we designed coupon tests for the provided composite and static and dynamic drop tests for the landing gear. Additionally, we designed the drop test apparatus that was used to collect this data and decided upon the necessary electronics for accurate data collection. The final aspect of this project was to provide M-Fly with a finite element model (FEM) for use in future design and selection of landing gear. Testing occurred in the Aerospace 405 work area in an efficient manner throughout the course of the three-month long project. In addition, we utilized testing facilities from Professor Henry Sodano of the Aerospace Materials Lab. Our team of five engineers, working with a consultant, have completed the project by April 28th, 2019 for your review and dissemination to future leadership. You would be pleased to learn that we completed this study for under \$80,000.

We thank you for providing us with the aluminum landing gear for initial testing, the carbon fiber fabric, and the 80/20 aluminum framing used for the drop test apparatus. Thank you for the opportunity.

Sincerely,

Amanda Jackson (Team Leader)

Mario Alvarez Anjali Balani

Emily Kusulas Changqing Lu

enc.



Final report: Structural testing and
analysis of aluminum and composite
landing gear

Final report: Structural testing and analysis of aluminum and composite landing gear



April 26, 2019

Authors:
Amanda Jackson, Lead Engineer
Mario Alvarez
Anjali Balani
Emily Kusulas
Changqing Lu

Recipient:
Philip Wdowiak
M-Fly Team Captain

Contents

| | |
|--|-----------|
| Acronyms and Abbreviations | iv |
| 1 Executive Summary | 1 |
| 2 Introduction | 1 |
| 3 Overview of Tasks | 2 |
| 4 Criteria | 2 |
| 5 Support | 3 |
| 5.1 Method | 3 |
| 5.1.1 Carbon Fiber Landing Gear Production | 3 |
| 5.1.2 Finite Element Model | 4 |
| 5.2 Testing | 5 |
| 5.2.1 Carbon Fiber Coupon Testing | 5 |
| 5.2.2 Pendulum Testing | 8 |
| 5.2.3 Drop Test | 9 |
| 5.2.4 Deflection Test | 10 |
| 5.3 Results | 10 |
| 5.3.1 Results of Coupon Testing | 10 |
| 5.3.2 Results of Pendulum Testing | 11 |
| 5.3.3 Results of Drop Tests | 12 |
| 5.3.4 Results of Deflection Tests: | 13 |
| 5.3.5 Abaqus Results: | 15 |
| 5.4 Analysis | 15 |
| 5.4.1 Coupon Testing Result Analysis | 15 |
| 5.4.2 Pendulum Testing Result Analysis: | 16 |
| 5.4.3 Drop Test Result Analysis: | 17 |
| 5.4.4 Deflection Test Result Analysis: | 17 |
| 5.4.5 Abaqus Result Analysis: | 17 |
| 6 Omissions and Limitations | 18 |
| 7 Conclusion | 19 |
| 8 Cost and Schedule | 19 |
| Appendix | 22 |
| A Figures | 22 |
| A.1 Abaqus Model | 22 |
| A.2 Pendulum Test Raw Data | 24 |
| A.3 Tensile Test Raw Data | 25 |
| A.4 Drop Test Sample Data | 26 |

| | |
|--|-----------|
| B Tables | 27 |
| B.1 Four-Point Bending Test: Specimen Measurements | 27 |
| B.2 Drop Tests: Impact Times | 28 |
| B.3 Tensile Tests: Specimen Measurements | 28 |
| C Drop Test Derivation | 28 |
| D Codes | 29 |

List of Figures

| | | |
|----|--|----|
| 1 | CNC Schematic | 4 |
| 2 | Carbon Fiber Landing Gear Mold | 4 |
| 3 | Abaqus Models | 5 |
| 4 | Carbon Fiber Configuration | 6 |
| 5 | Carbon Fiber Cure | 7 |
| 6 | Carbon Fiber Coupon Test | 8 |
| 7 | Pendulum Test | 8 |
| 8 | Drop Test Setup | 9 |
| 9 | Landing Gear Deflection | 10 |
| 10 | Damping Ratio Example | 12 |
| 11 | Drop Test Impact Force | 13 |
| 12 | Horizontal Deflection | 14 |
| 13 | Vertical Deflection | 14 |
| 14 | Carbon Fiber Displacement at 60-lb Load | 15 |
| 15 | Gantt Chart | 19 |
| 16 | Abaqus model at MTOW- deformation | 22 |
| 17 | Carbon fiber has lower stresses than aluminum landing gear at MTOW | 23 |
| 18 | Pendulum Test Raw Data at $L_1 = 12.75\text{in}$, $\theta = 10^\circ$ | 24 |
| 19 | Pendulum Test Raw Data at $L_1 = 10.25\text{in}$, $\theta = 10^\circ$ | 24 |
| 20 | Tensile Test Raw Data | 25 |
| 21 | Tensile Test Raw Data at Failure | 26 |
| 22 | Drop Test Sample Data | 26 |

List of Tables

| | | |
|----|---|----|
| 1 | Errors reported with 90% confidence are below 15% | 11 |
| 2 | Pendulum Dampening Ratio and Period Results | 12 |
| 3 | Impact force results have % error of 4% | 13 |
| 4 | Material Properties from Coupon Testing | 16 |
| 5 | Coefficients of Determination for Deflection | 17 |
| 6 | Material Costs | 20 |
| 7 | Total Cost | 20 |
| 8 | Four-Point Bending Test Raw Data | 27 |
| 9 | Tensile Test Results | 27 |
| 10 | Four-Point Bending Test | 27 |
| 11 | Drop Test Results for Landing Gear of Two Materials | 28 |
| 12 | Tensile Tests | 28 |

Acronyms and Abbreviations

ASTM: American Society for Testing and Materials

CAD: Computer Aided Design

CLT: Classical Lamination Theory

CNC: Computer Numerical Control

DAQ: Data Acquisition System

FEA: Finite Element Analysis

FEM: Finite Element Model

FRF: Frequency Response Function

g: gravitational acceleration

MTOW: Maximum TakeOff Weight

RC: Radio Controlled

SAE: Society of Automotive Engineers

1 Executive Summary

M-Fly is investigating using a composite landing gear on its advanced-class aircraft. They have requested that we analyze and compare the performance of its previously-used aluminum landing gear to the composite landing gear. We have been asked to provide a final recommendation on which material to use for future landing gear designs. This set of experiments is important because a hard landing can be the fastest way to destroy months of hard work on an aircraft. To combat the high loads experienced during a hard landing, hobbyists usually increase the thickness or add braces to increase landing gear strength. However, these methods increase weight, thereby limiting aircraft performance. Since M-Fly competes in competitions where 55 pounds is the MTOW limit, the additional weight caused by metal landing gear can adversely affect the score received. Consequently, our study of carbon fiber landing gear will provide M-Fly with a viable alternative to regular carbon fiber. To keep abreast of our investigation, M-Fly requested a final report on our testing apparatus, experimental data, and conclusions. In response to M-Fly's request, we have successfully designed and tested a drop test rig and we have collected data on both the conventional and composite landing gear. The composite landing gear weighs 0.76 lb with wheels, whereas the aluminum landing gear weighs 0.96 lb with wheels. The purpose of this report is to provide an overview of our experiment setup, methods, and analysis of our data and to offer recommendations on landing gear design and testing for M-Fly's future aircraft.

Having completed analysis of our composite and aluminum landing gear, we have concluded that due to its material strength and lightness, the composite is a superior alternative to the existing aluminum structure. We thus recommend the carbon fiber design. We have compiled our analyses into a finite element model which can be used to perform future analysis on the design.

This project is feasible because it can be completed in the allotted time of three months and in the provided physical space of a 2.5-foot-by-4-foot lab table. Our main drop test setup and methodology is desirable because it is repeatable; we have validated that there is an error of less than or equal to 10% with at least 80% confidence in a given set of tests. To further support the desirability of the tests, we have also confirmed that the accelerometer is accurate to within 3% error or less. The project is affordable because we have spent less than the \$400 budget provided for testing. Finally, we have set a preferability criterion based on team expertise and carbon fiber properties. Our team members have expertise in the different areas necessary for successful testing. The strength properties of the carbon fiber are greater than the strength properties of 6061 aluminum. Thus, team expertise and carbon fiber testing results both satisfy the desirability criterion.

2 Introduction

Composite materials such as carbon fiber reduce the weight of a component while providing the necessary strength and stiffness properties needed for successful flight. Because of its potential to reduce airframe weight, composite technologies have been the focus of many advancements within the aerospace industry. However, the complex structure of carbon fiber and composite materials creates challenges in understanding structural performance. Due to lack of knowledge and time limitations, M-Fly has not designed a composite landing gear structure, opting for a store-bought aluminum landing gear instead. In efforts to increase the strength properties of the landing gear, gussets and thicker metal is utilized. However, these methods increase weight, thereby limiting

aircraft performance. This is a problem for RC enthusiasts as well. As hobbyists, there is limited time and resources for trying new solutions. This semester is the first time that M-Fly will be attempting to use a carbon fiber component, but it is unsure of how it will perform during rough landings. Our analysis of carbon fiber landing gear performance in a drop test will allow the M-Fly project team members to explore and understand new design spaces and consequently, create more efficient aircraft. Consequently, our study of carbon fiber landing gear will provide the larger RC enthusiast community with aircraft that are both robust and high-performance.

While the study of composite materials is a topic of many structures research labs, there is little documentation for small-scale RC aircrafts. Thus, it was necessary to conduct extensive research into composites, as well as to perform many tests to better understand the exact behaviors of the composites we are testing with. Composites structures can meet load-bearing and safety factor criteria while exacting a much lower weight penalty on the entire system, making them highly desirable. Mangalgi [10] explored the scope of composites in aerospace applications. Landing gear experience large impact loads and stresses and its failure can fatally compromise the entire structure. Guimbal [6] developed composite landing gear capable of supporting impact loads for full scale aerostructures such as helicopters. However, such landing gear has not been adapted for smaller systems such as drones or RC aircraft, nor has it been compared to traditional, metal landing gear. We plan to assess the benefits of changing the material via drop tests on the respective materials and landing gear. Howell et al [8] performed drop testing on composite landing gear with active control to reduce the loads transmitted to the entire airframe, which is outside of the scope of this experiment, but could offer additional information to the importance of a robust landing gear analysis. M-Fly has expressed interest in building their own carbon fiber landing gear; based on our experimental findings, we recommend that they move forward with this endeavor.

3 Overview of Tasks

In order to accurately compare the aluminum landing gear to the composite landing gear, we performed four different tests. First, we tested the structural properties of a set of ten 15-ply carbon fiber coupons by conducting tensile and four-point bending tests. We conducted pendulum tests to validate the readings from the accelerometer used in the drop tests. We then dropped the landing gear from different heights to determine the loads the structures experienced. We then conducted deflection tests that allowed us to understand how a given load on the structure would deflect it horizontally and vertically. Finally, we inputted the deflections as into Dassault Systemes' Abaqus as boundary conditions and ran simulations to provide M-Fly with the ability to run similar tests with less money and time committed.

4 Criteria

We used various criteria to plan the project and to validate our testing methodology. We chose the most important of these criteria to be feasibility. We evaluated if this criterion was met based on the following two metrics: whether our experiment fit in the time required to complete the project and whether it fit in the physical facilities provided. The benchmark for experiment time frame is the three months in a semester. For physical space, the benchmark is the 2.5-foot-by-4-foot size of the lab table.

The next most important criterion is desirability. A metric for this criterion is reliability of our accelerometer readings. Our metric is the percent error between theoretical acceleration and tested acceleration reading, and our benchmark is a percent error of 3% or less. Another metric for this criterion is whether the carbon fiber is stronger than the aluminum. The benchmark for this is if the carbon fiber's maximum flexural strength and maximum tensile strength are greater than the aluminum's tensile yield strength. Our final metric for desirability is weight; if the carbon fiber landing gear is lighter than the aluminum, then it is desirable.

The third criterion is affordability. Our metric for this criterion is cost of materials and our benchmark to be satisfied is the \$400 budget for the whole project.

The final criterion is preferability. Our project will be preferable if our team members have experience and interest in the four major disciplines required: frame assembly, electronics, composite layups, and FEA simulations. Our benchmark is at least each member has experience in at least one of these disciplines. This was satisfied by diverse, prior work experience of the team with the different aspects of the project which span data collection, composite materials, setup of the test rig, etc. This was further satisfied by judging the preferability of the chosen apparatus which included the electronics as well as building materials chosen. Our data collection method is preferable because Raspberry Pi has extensive information available to help with troubleshooting.

5 Support

This section details methods used, testing conducted, results recorded, and the analyses done on the results.

5.1 Method

This section details processes, such as production strategies, that aided in test setups and post-testing analysis.

5.1.1 Carbon Fiber Landing Gear Production

The composite landing gear mold was machined using the ShopBot CNC router in Professor Washabaugh's 205 lab, which can be seen in Figure 1. This method of making the mold was preferred due to the team member's experience with working in CATIA V5 and due to Professor Washabaugh's excellent documentation on generating female molds and toolpaths. The mold proved to be a time-consuming task because of the complexity of the shape, compared to the hovercraft shells typically manufactured in the lab. Thus, we ended up machining the female mold so that we could perform the layup by draping the easy-to-cut, 3.25" x 30" strips over its top surface, as shown in Figure 2.

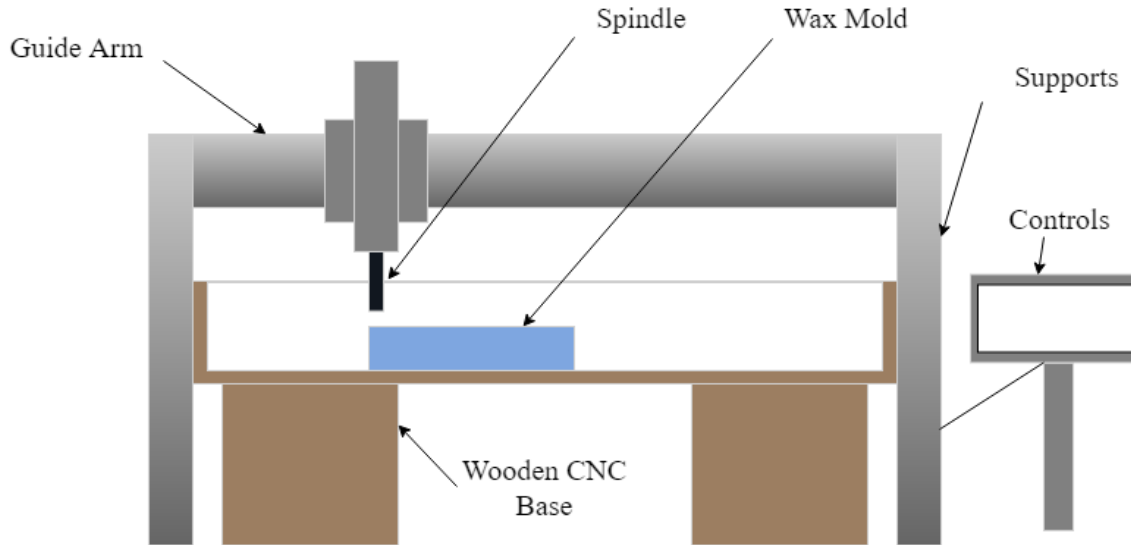


Figure 1: CNC uses a drill bit and spindle to cut and moves along a guide arm



Figure 2: Female mold for landing gear layup cut with the CNC ShopBot

The layup was performed using the same $[0/90\ 45\ 0/90\ 45\ 0/90\ 0/90\ 0/90\ 0/90\ 0/90\ 0/90]$ $[0/90\ 45\ 0/90\ 45\ 0/90]^{\circ}$ ply pattern used to fabricate the carbon fiber coupons. After curing in vacuum for 12 hours, the landing gear was demolded and trimmed to the designed geometry. With wheels attached, the carbon fiber landing gear is 0.76 lbs and the aluminum with wheels attached is 0.96 lbs. The carbon fiber landing gear is lighter than the aluminum, so our desirability criterion is met.

5.1.2 Finite Element Model

Abaqus is a program that is used to conduct finite element analysis and it is particularly useful because it can model composite materials. Modeling composites is typically very difficult because

the fibers run in different directions. As a result, the composite will have different properties in tension, compression, and shear. The finite element method is a method used to approximate governing equations to help solve complex problems with an infinite number of unknowns. It utilizes the Galerkin approach, with takes the strong form of a differential equation and converts it to the weak form using interpolation points [13]. To simulate the behavior, a CAD model was created in SolidWorks with no material assigned to the part. The part was then imported into Abaqus where we applied the material properties of the composite and the aluminum.

In Abaqus, we applied boundary conditions to the landing gear models as seen in Figure 3a. The decision to use boundary conditions instead of loads was due to the explicit nature of our program. After making our original model, it was suggested that using an explicit model to represent a static problem as a dynamic one would help to reduce run time and to increase the fidelity of our results. A FEM uses nodal elements and interpolation points to create meshes, or localized sections of the material, as seen in Figure 3b. Having smaller meshes is useful because it helps to refine the fidelity of the simulation. Once the simulation is complete, we are able to find the value and location of the maximum stress experienced by the structure.

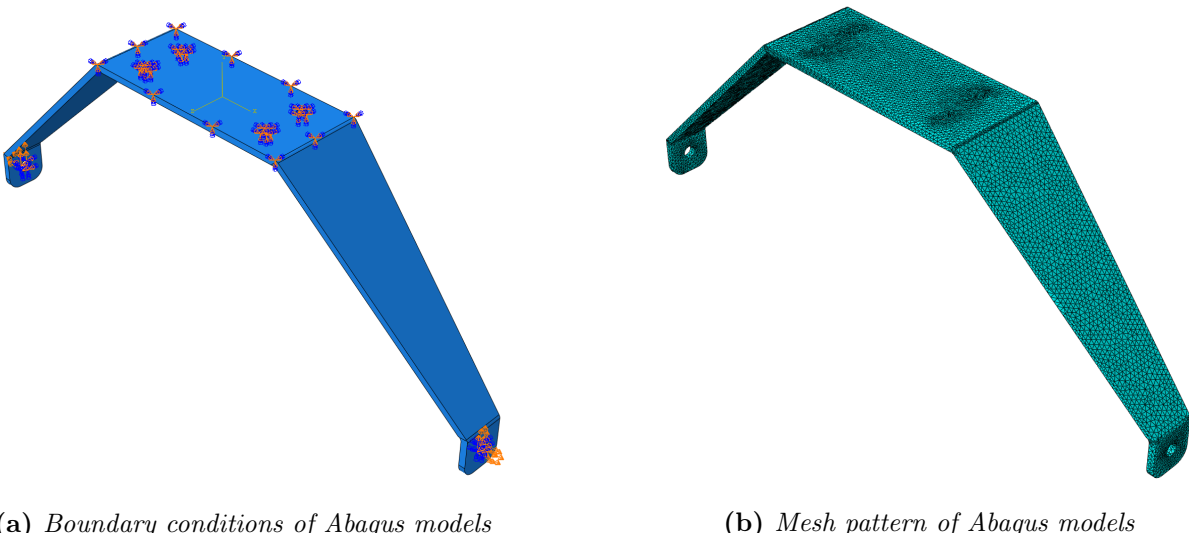


Figure 3: Explicit Abaqus models utilize boundary conditions and mesh

5.2 Testing

This section presents all the tests conducted throughout the project.

5.2.1 Carbon Fiber Coupon Testing

Coupon Layup: We decided to manufacture carbon fiber test coupons in order to conduct destructive four-point bending and tensile tests. The results of these tests could be used to validate the theoretical strength properties of a 15-ply carbon fiber composite.

We chose to manufacture a landing gear from 15 plies of carbon fiber because it would most closely mimic the aluminum landing gear's thickness of 0.125 inches. Thus, we made a design choice to match the geometry of our aluminum part, rather than its structural properties. Composites can

be designed for optimal performance by changing the angles of each ply. The fabric we are using has fibers running in the 0- and 90-degree directions. By rotating the fabric by 45 degrees, we are able to obtain strength properties in different directions, increasing the structure's strength in shear and flexure, as shown in Figure 4.

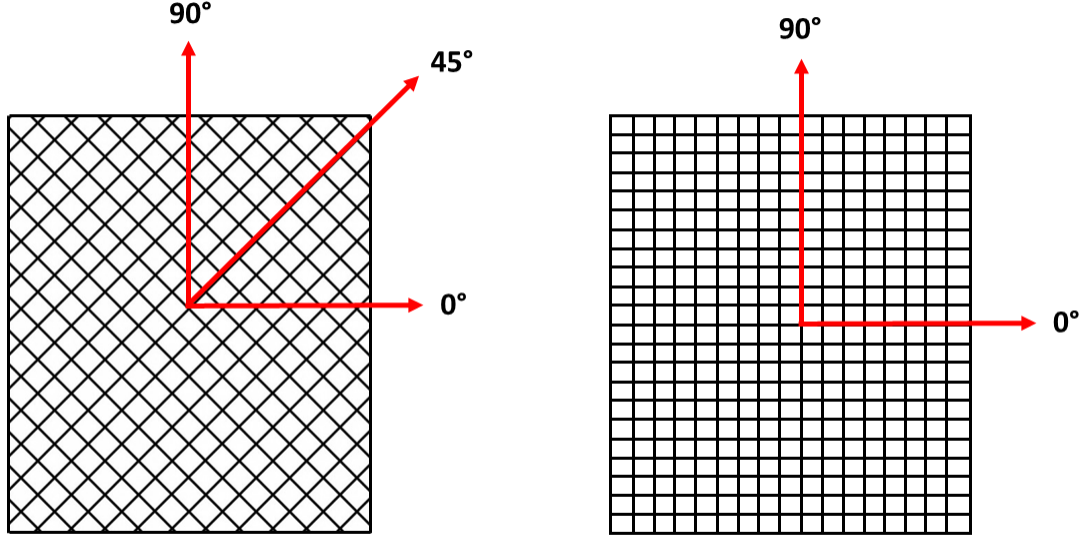


Figure 4: 45° (left) and $0 - 90^\circ$ (right) ply configurations give strength in multiple directions

The $[0/90\ 45\ 0/90\ 45\ 0/90\ 0/90\ 0/90\ 0/90\ 0/90\ 0/90\ 0/90\ 0/90\ 45\ 0/90\ 45\ 0/90]^\circ$ ply pattern was determined using classical lamination theory (CLT) [7], a method of calculating the theoretical strength properties of a composite laminate based on its fiber orientations. The code for this calculation can be found in the Appendix. This method is reliable for understanding the best orientations of each ply, but it is not representative of multidirectional fabrics. As a result, we do not derive any expected strength properties from CLT.

In order to make the composite part, we needed to conduct a wet layup in which the dry fabric was imbued with a West Systems epoxy resin system used by M-Fly. After conducting the wet layup in the M-Fly area, we erected a vacuum bag around the laminate to ensure that the resin infiltrated as much of the fabric as possible. Figure 5 shows the laminate curing under vacuum and the finished part.

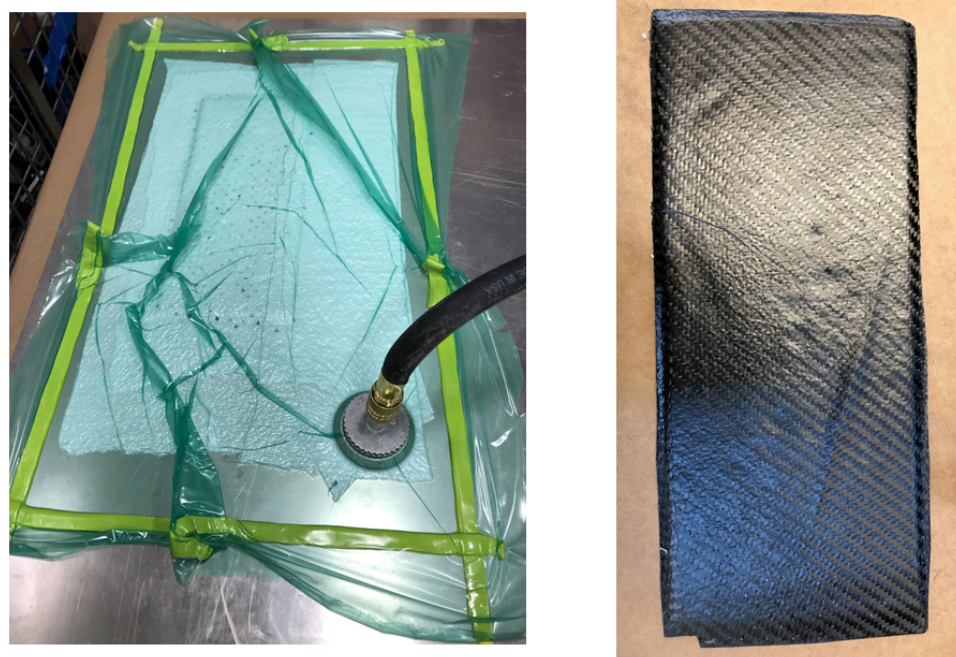


Figure 5: Vacuum cure process (left) creates finished carbon fiber part (right)

The finished laminate was then cut using the diamond saw in Professor Sodano's lab space, creating ten coupons, or test specimens with which to test our material properties. For all testing, we used a 5982 Series Instron Electromechanical Testing System. Five of these specimens were tested to failure in a four-point bending test, as shown in Figure 6b. The other five test specimens were tested in a destructive tensile test, as shown in Figure 6a. To ensure that we conducted each test correctly, we followed procedure in ASTM D7264, "Standard Test Method for Flexural Properties of Polymer Matrix Composite Materials" and in ASTM D3039, "Standard Test Method for Tensile Properties of Polymer Matrix Composite Materials."

Test Setup: To test the material characteristics of the carbon fiber coupons, we conducted the four-point flexural bending test and the tensile test to measure the flexural elasticity modulus and the tensile modulus. The test setup are shown in Figure 6.

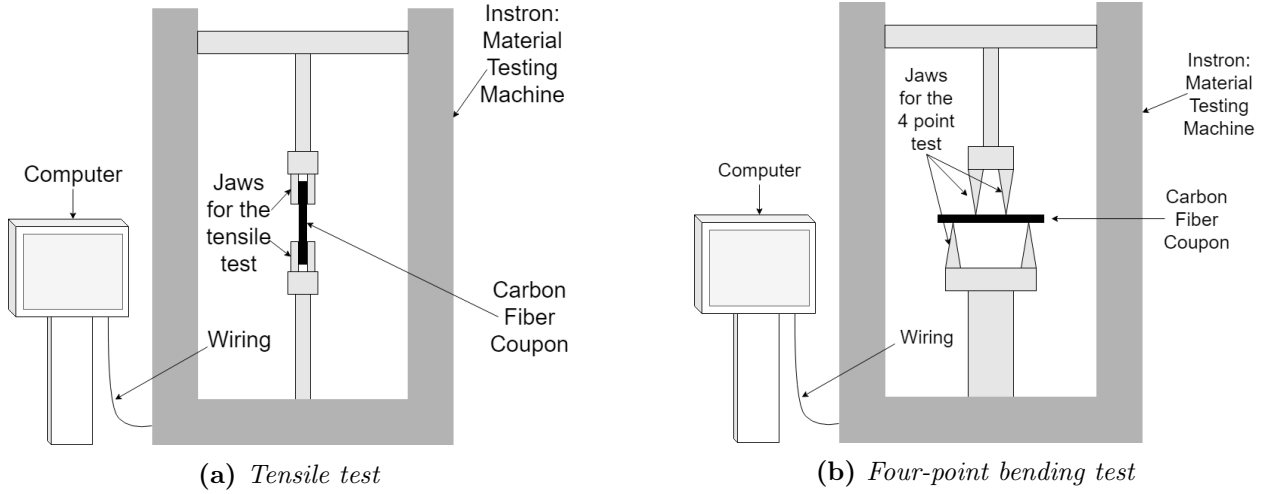


Figure 6: Schematic shows carbon fiber coupon testing configuration

5.2.2 Pendulum Testing

Test Setup: One of the main goals of the experimentation was to measure the acceleration of the landing gear during fall and at impact. The data acquisition system consisting of the Raspberry Pi and the Adafruit MMA8451 accelerometer needed validation before being implemented for drop tests. In order to accomplish this, we setup a pendulum configuration shown in Figure 7a and compared the theoretical results of the period T of the pendulum to the experiment results measured using the accelerometer. The Raspberry Pi and the accelerometer are integrated in the configuration shown in Figure 7b. The accelerometer is attached to a breadboard which is connected to the back of the Raspberry Pi.

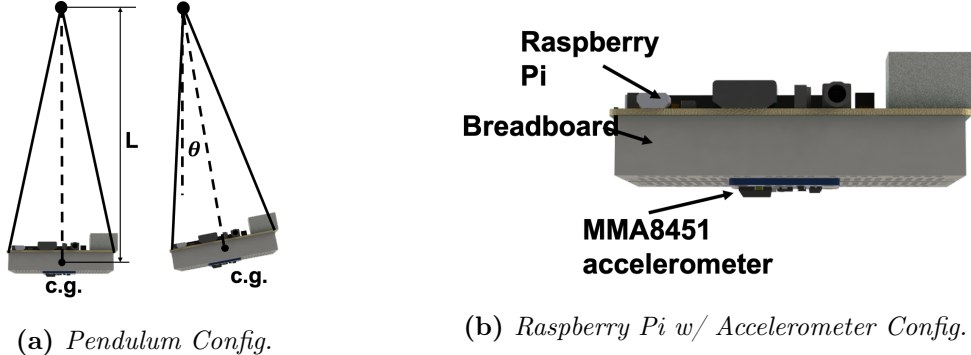


Figure 7: Pendulum test validates the readings of the data acquisition system of the Raspberry Pi and Adafruit MMA8451 accelerometer

Based on the setup, we approximated the block consisting of the Raspberry Pi, breadboard and the accelerometer as a point mass. Furthermore, the initial angle of displacement θ was assumed to be small enough for the small angle approximation to hold. Based on these two assumptions, we can approximate the setup as a simple pendulum to calculate the period of oscillation. Thus, the theoretical period T of such a simple pendulum with a string length L is,

$$T = 2\pi \sqrt{\frac{L}{g}}, \quad (1)$$

where g is the local acceleration due to gravity. Note that this equation is an oversimplification of a much more complicated problem.

For each test, we set the initiation angle θ at 10° , recorded the pendulum length L and used the Raspberry Pi to record the acceleration of z -axis, a_z , in m/s^2 and the time t in seconds.

5.2.3 Drop Test

Test Setup: In order to mimic the landing scenario for the actual plane from M-Fly, we designed a rotating 80/20 beams with L-bracket connections for the drop test. The schematics are shown on Figure 8.

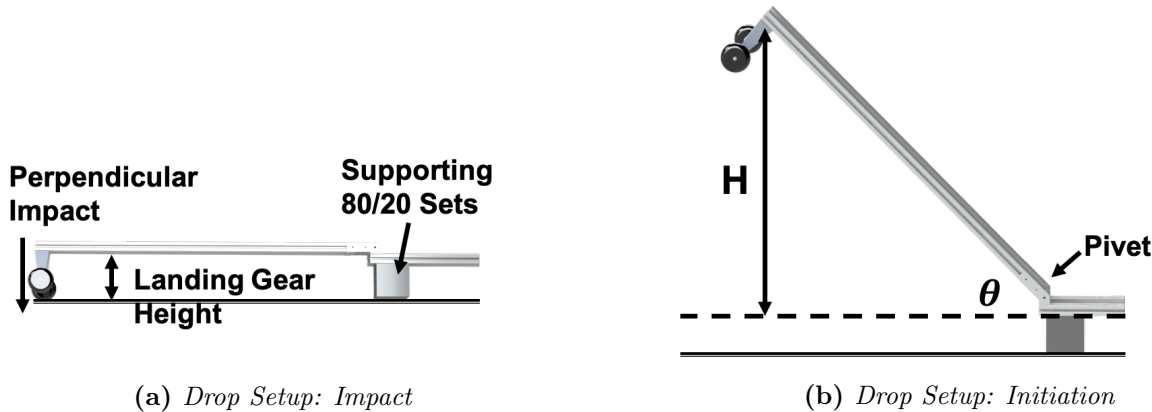


Figure 8: Drop test setup with supporting 80/20 beam structure ensures perpendicular impact of the landing gear on the ground

As we can see on Figure 8a, the landing gear is connected to the 80/20 beams perpendicularly. Another set of 80/20 beams are fixed on a set of 80/20 beam structures with the same height of the landing gear so that when dropped, the landing gear can impact the ground with a downward velocity. It is important to make sure that the landing gear is dropped with a downward impact velocity since we are interested in the acceleration in the z -axis direction as well as the impact force on the landing gear. The shape of the landing gear is most susceptible to the impact directly from the ground because there might be stress concentration on the flare part of the landing gear.

Note that the swinging setup involves the 80/20 beams rotating downwards together with the landing gear. Therefore, the rotating 80/20 beams also contribute to the impact force on the landing gear as an equivalence of an additional mass. We first measure with no mass added and calculate the impact force contributed by the rotating 80/20 beams according to the derivation in Section C.

In order to mimic the real landing scenario, we also need to conduct drop test with varying mass added onto the landing gear. Theoretically, as the mass of the landing gear increases, the impact time will increase. The increase in impact time can alleviate the maximum impact force on the landing gear, thus decreasing the stress concentration on the flare part.

5.2.4 Deflection Test

Test Setup: The impact time, masses placed on the swinging arm, and the test setup measurements can be used in Equation 13, which is derived according to the content of Appendix C. Equation 13's output is the average force experienced by the landing gear at maximum acceleration. In order to find the resultant deflections in the structure at these calculated loads, we placed masses on the top portion of the landing gear, mimicking the support that a small aircraft's chassis would provide along that section. Under these loads, the landing gear experienced horizontal and vertical deflection, as shown in Figure 9.

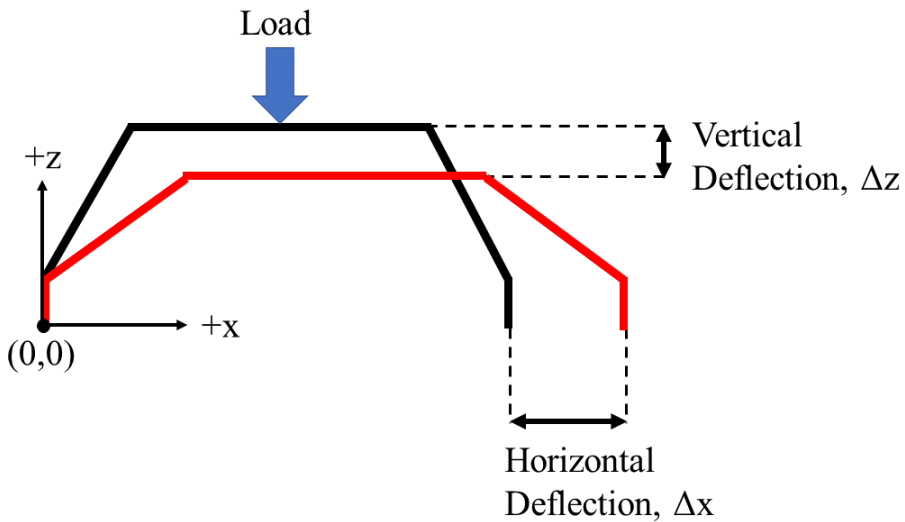


Figure 9: Landing gear deflects horizontally and vertically when loaded

We measured the Δx and Δy of both the carbon fiber and aluminum structures by securing them to a wall at the origin, as shown in 9. The structure was not allowed to rotate or move at that point. We then greased an aluminum sheet with white lithium grease to ensure that landing gear structures could deflect as frictionlessly as possible. Each structure was loaded up with three different weights. These weights ranged from 0.5 pounds to two pounds and they were placed incrementally onto the top surface of the structure to ensure that the structure didn't flex suddenly. When the total weight was added, the vertical and horizontal deflections were recorded. These deflections were inputted into the Abaqus model as boundary conditions.

5.3 Results

This section presents all the results for the testing completed.

5.3.1 Results of Coupon Testing

Each ASTM also instructed us how to process the data that we collected in each test; we followed Calculation 13.2 for maximum flexural stress and Calculation 13.7.2 for flexural secant modulus of

elasticity in ASTM D7264 and Calculation 13.3 for maximum tensile stress and tensile modulus of elasticity in ASTM D3039. The results of these tests can be found in Table 1.

Table 1: Errors reported with 90% confidence are below 15%

| Material Property | Carbon Fiber | Error with 90% |
|--------------------------------------|--------------|----------------|
| Maximum Flexural Stress [MPa] | 504.24 | 0.0606 |
| Flexural Modulus [GPa] | 55.32 | 0.0276 |
| Maximum Tensile Stress [MPa] | 560.47 | 0.0683 |
| Young's Modulus [GPa] (tensile test) | 6.33 | 0.1252 |

The tensile test records the time t , the load on specimen as well as the extension of the specimen. The raw data plot is presented in Section A.3. After fitting the elastic region of the curve, we calculated the tensile modulus of five coupons respectively. The results are in Table 9 below. The average results for the material properties are presented in table 1. We were not able to collect data on maximum tensile stress for the carbon fiber coupons because the Instron was incapable of breaking a laminate with a thickness of 0.125 inches. As a result, we do not have these numbers available; the Omissions and Limitations section contains further discussion of the tensile tests.

All the values reported in Table:1 are the mean values for the processed target value. The accuracy of each mean value was calculated using the standard error of the target value and the z-score for the 90th percentile as shown below.

$$\text{standard error}, \bar{\sigma} = \frac{\sigma}{\sqrt{N}} \quad (2)$$

$$\text{accuracy} = \frac{1.645 \times \bar{\sigma}}{\text{mean}} \quad (3)$$

5.3.2 Results of Pendulum Testing

For each test, we obtained the damping ratio ϵ , the pendulum period T and the average z -axis acceleration \bar{a}_z from raw data (Section A.2).

The process of approximating the damping ratio is shown in Figure 10. After plotting the raw data, we used the exponential decaying envelope $Me^{-\epsilon t}$ to enclose the decaying raw data, where M is a scaling factor for the magnitude. In Figure 10, the damping ratio ϵ is approximately 0.27.

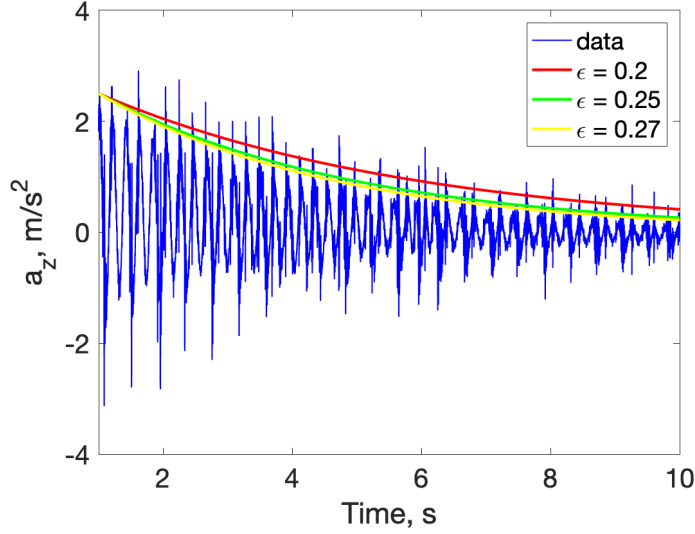


Figure 10: Pendulum tests result in damping ratio of $\epsilon \approx 0.27$.

To calculate the period for each case, we counted the number of peaks within a certain time range. The number of periods within the time range is half of number of peaks. The averaged period is,

$$T_{exp} = \frac{\text{total time}}{\# \text{ of periods}} \quad (4)$$

We set up two configurations, with $L_1 = 12.75 \text{ in}$ and $L_2 = 10.25 \text{ in}$. The processed results are shown in tables 3a and 3b.

Table 2: Damping ratio and period results from pendulum test

| Test | ϵ | T (s) | Avg. Acc (m/s^2) |
|------|------------|-------|----------------------|
| 1 | 0.35 | 0.45 | 9.72 |
| 2 | 0.24 | 0.44 | 9.78 |
| 3 | 0.20 | 0.46 | 9.78 |
| Avg. | 0.26 | 0.45 | 9.76 |

(a) $L_1 = 12.75 \text{ in}, \theta = 10^\circ$

| Test | ϵ | T (s) | Avg. Acc (m/s^2) |
|------|------------|-------|----------------------|
| 1 | 0.40 | 0.41 | 9.62 |
| 2 | 0.50 | 0.40 | 9.71 |
| 3 | 0.27 | 0.41 | 9.86 |
| Avg. | 0.39 | 0.41 | 9.73 |

(b) $L_2 = 10.25 \text{ in}, \theta = 10^\circ$

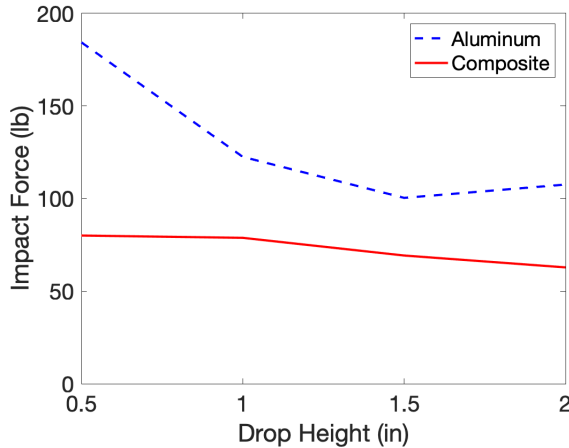
5.3.3 Results of Drop Tests

As we can see from Table 11, the values of impact time are readings from the raw data plot (Section A.4). And based on the analysis discussed in Section C, we can calculate the impact forces at different heights. The results are shown in Table 3.

Table 3: Impact force results have % error of 4%

| Height (in) | Aluminum Impact Force (lb) | Composite Impact Force (lb) |
|-------------|----------------------------|-----------------------------|
| 0.5 | 368.19 ± 14.73 | 160.10 ± 6.40 |
| 1.0 | 244.73 ± 9.89 | 157.48 ± 6.30 |
| 1.5 | 200.76 ± 8.03 | 138.42 ± 5.54 |
| 2.0 | 215.25 ± 8.61 | 125.59 ± 5.02 |

We can see the performance for two landing gears from the following Figure 11.

**Figure 11:** Impact force experienced by the composite landing gear is lower than the aluminum landing gear when dropped at same height

To find the deflection that would be inputted into our Abaqus model, we selected the force experienced at the highest drop height recorded. See the Limitations and Omissions section for further discussion.

5.3.4 Results of Deflection Tests:

To process our deflection test results, we recorded three data points of vertical or horizontal deflection against load in pounds of force. We then prescribed a line of best fit to these data points. Because we are dealing with stresses that reside in the elastic regime, we can extrapolate beyond the range of data points collected. The horizontal deflection is plotted against load for both landing gear in Figure 12. Similarly, Figure 13 depicts the vertical deflection plotted against load for both structures.

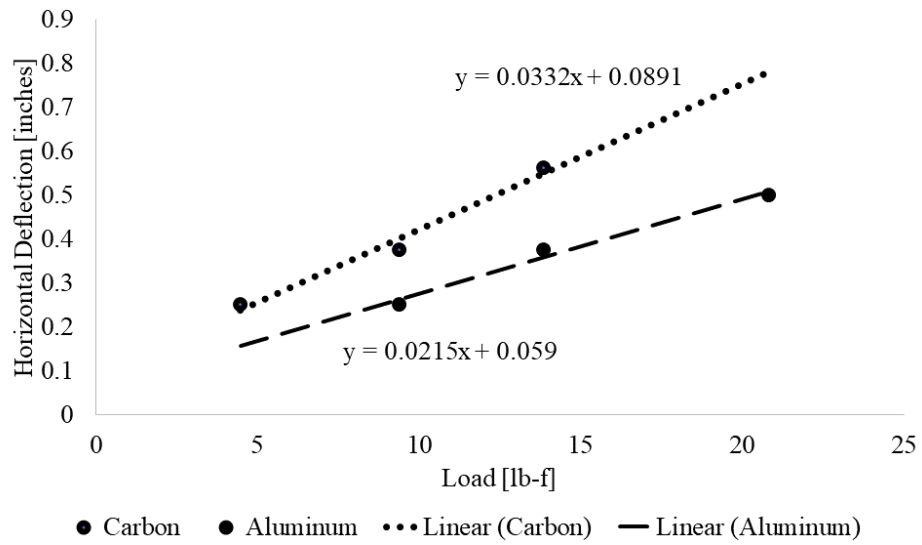


Figure 12: The carbon landing gear deflects vertically more than the aluminum at a given load

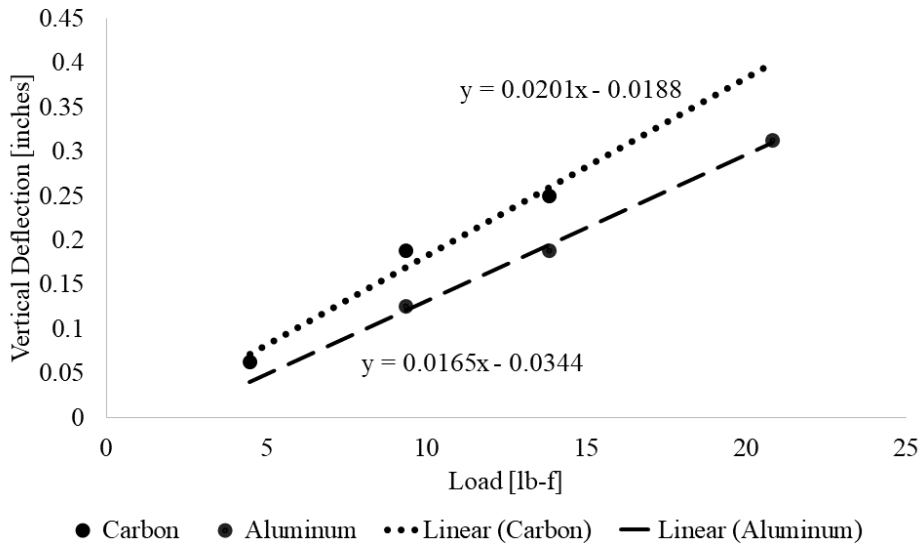


Figure 13: The carbon landing gear deflects vertically more than the aluminum at a given load

We have four equations for the lines of best fit for the sets of deflection data. The x in each equation corresponds to the load on the landing structure in pounds-force. Likewise, the y in each equation refers to the horizontal or vertical deflection, in inches. Given the force calculated from our drop

test results, we can find the resultant deflection in the structure with these equations for the lines of best fit. Because we are assuming that the resultant stresses do not cause plastic deformation or fracture in the aluminum and carbon fiber, respectively, we can extrapolate these weights and deflections beyond the range of values tested.

5.3.5 Abaqus Results:

We are able to visualize the expected deformation that the landing gear experiences when landing. Figure 14 shows the stresses that the landing gear undergoes when it is loaded during landing as well as the shape of the deformation.



Figure 14: At 60-lb load, the carbon fiber landing gear deforms compared to the unstressed structure

5.4 Analysis

This section presents Presented here is the analysis of all the data collected.

5.4.1 Coupon Testing Result Analysis

To analyze the results of our coupon testing, we compare to known strength properties of 6061 aluminum, the material against which we will be comparing our composite landing gear. The standard strength properties of 6061 aluminum are found in Table 4. Note that we can compare the tensile properties of aluminum to both the tensile and flexural properties of carbon fiber. Aluminum will fail through yielding, which occurs after plastic deformation due to tension or bending (flexure). If we approximate our multidirectional carbon fiber as quasi-isotropic, we can compare its flexural and tensile properties to that of aluminum. Because we are concerned with whether our carbon

fiber landing gear is preferable to the conventional aluminum landing gear, we compare the average strength properties from coupon testing with their equivalent properties for aluminum. We can see from Table 4 that our tested elastic modulus is less than the elastic modulus of aluminum, indicating that the aluminum is stiffer than carbon fiber. However, in tension and flexure, carbon fiber will fail at a higher stress than aluminum; thus, the carbon fiber is stronger. Thus, our desirability criterion is met for carbon fiber material properties.

Table 4: The carbon fiber layup is stronger and more flexible than 6061 aluminum

| Material Property | Carbon Fiber (tested) | 6061 Aluminum (standard) |
|--------------------------------------|-----------------------|--------------------------|
| Maximum Flexural Stress [MPa] | 504.24 | 310.00 |
| Flexural Modulus [GPa] | 55.32 | 68.90 |
| Maximum Tensile Stress [MPa] | 560.47 | 310.00 |
| Young's Modulus [GPa] (tensile test) | 6.33 | 68.90 |

5.4.2 Pendulum Testing Result Analysis:

It is seen in Table 2 that the pendulum test consisted of 3 trials for each pendulum length L . For each length, we can see that the pendulum periods from three trials are approximately the same, which confirms the repeatability of the data acquisition process. Although the damping ratio ϵ for each trial was found to be quite different, the damping of each trial does not influence the period significantly.

For the theoretical pendulum period calculated from Equation 1, we have,

$$\begin{aligned} T_{1,\text{theo}} &= 2\pi \sqrt{\frac{L_1}{g}} = 2\pi \sqrt{\frac{12.75 \times 0.0254}{9.78}} = 1.14 \text{ s}, \\ T_{2,\text{theo}} &= 2\pi \sqrt{\frac{L_2}{g}} = 2\pi \sqrt{\frac{10.25 \times 0.0254}{9.78}} = 1.02 \text{ s}. \end{aligned} \quad (5)$$

The theoretical values and experimental results are very different from one another, which indicates that the pendulum setup in Figure 7 can not be assumed to be a simple pendulum setup. However, the period T and the pendulum length L has a relationship where:

$$T \sim \sqrt{L}. \quad (6)$$

Therefore, we can compare the ratio of the experimental period results T_1/T_2 with $\sqrt{L_1/L_2}$, where from the experiment, we have,

$$\frac{T_1}{T_2} = 1.110 \approx \sqrt{\frac{L_1}{L_2}} = 1.115, \quad (7)$$

which implies that although the setup can not be assumed to be a simple pendulum, the period T and pendulum length L relationship is consistent. For L_1 and L_2 , the average z -axis accelerations are 9.76 m/s^2 and 9.73 m/s^2 respectively. The local acceleration due to gravity at the experiment location is 9.804 m/s^2 . The % error is,

$$\% \text{ error}_1 = 0.45\%, \quad \% \text{ error}_2 = 0.75\%, \quad (8)$$

which are less than our benchmark of 3%. Therefore, it validates the accelerometer and Raspberry Pi DAQ system and proves the repeatability of the measurements. Because our percent error is less than our benchmark, we satisfy the desirability criterion for the accelerometer.

5.4.3 Drop Test Result Analysis:

From Figure 11, we can see that when dropped from same height, the composite landing gear experienced less impact force than the aluminum landing gear. Generally, the impact force we calculated results from the force to stop the downward velocity of the landing gear. To decrease the downward velocity v , an impact force exert on the landing gear (both wheels) during a impact time Δt .

If the landing gears are dropped at the same height, the downward velocity before impact should be the same for both landing gears. Therefore, according to the conservation of momentum, with less impact time, the greater the impact force. The results show that the composite landing gear has structural performance that leads to longer impact time. Therefore, composite landing gear produces less impact force shock to the whole structure of the aircraft.

With a percent error of 4%, the data shows good repeatability. And based on the calculation, composite landing gear produces less shock of impact force compared to aluminum landing gear when dropped at the same height. Therefore, the composite landing gear is structurally favored.

5.4.4 Deflection Test Result Analysis:

We can observe that the carbon fiber landing gear deflects more than the aluminum at a given load. The coefficient of determination, R^2 can be used to determine how well the line of best fit explains the variability of the data around its mean. The closer the R^2 value is to ± 1 , the better the linear model fits the set of data. Using MS Excel, we calculate the coefficients of determination for each of the four lines of best fit, recorded in Figure 5.

Table 5: High coefficients of determination indicate a well-fitting linear model

| Deflection Data | Coefficient of Determination (R^2) |
|---------------------------------|--|
| Vertical Deflection: Carbon | 0.9733 |
| Vertical Deflection: Aluminum | 0.9957 |
| Horizontal Deflection: Carbon | 0.9803 |
| Horizontal Deflection: Aluminum | 0.9846 |

All values of R^2 are less than 3% away from 100%. This indicates that for each set of data, only 3% of the variability is not explained by the linear model.

5.4.5 Abaqus Result Analysis:

Based on the results of our deflection tests, we ran the Abaqus model for the different loads experienced at the maximum drop height of 2 inches. Based on our analysis, there was a different

load for the aluminum and carbon fiber, thus warranting the different loads to be applied when landing. For the carbon fiber, this meant using displacements of (1.1872, 2.0811) inches in the x and y direction which is what can be expected at 60 lbs of force. For aluminum, displacements of (1.6981, 2.768) inches in the x and y direction were used which can be expected at 105 lbs of force. Based on our FEM, we can see that the maximum stress occurs at the location where the wheel is attached to the landing gear.

6 Omissions and Limitations

An omission from the original set of experiments is a rolling landing surface for the gear. This was originally going to consist of a motor connected to a belt that would allow for the landing gear to better simulate landing. However, changing the test setup to a swinging arm created space restrictions that did not allow the motor-driven belt to sit under the landing gear. In addition, the easiest way to purchase such an apparatus was to buy an old treadmill. However, this was no longer possible when we decided to use strain gauges to measure the loads applied; they are expensive and brought us too close to our 400 dollar budget to purchase our treadmill.

We were also limited by our composite lamination capabilities. M-Fly only possess dry carbon fiber and epoxy, as opposed to a pre-impregnated carbon fiber. Dry carbon fiber that undergoes a wet layup will generally have a lower fiber volume fraction and higher instance of air bubbles (known as voids), decreasing its strength properties. Because the fibers must be “painted” with epoxy resin, the fibers are also more likely to be misaligned during layup. This risk is heightened because the layup is occurring on a complex geometry. Fiber misalignment can also contribute to lower-than-expected strength properties. Finally, we noticed some dry spots on the laminates that we manufactured, indicating that the epoxy did not infiltrate all of the dry fibers. These factors led to lower strength properties than expected in our carbon fiber test specimens and in our composite landing gear.

During our tensile tests, the fiberglass tabs recommended by ASTM D3039 sheared off during testing. This was because the adhesive used to connect the fiberglass tabs had a lower shear strength than the tensile strength of the actual carbon fiber component. As a result, we have curve-fitted the initial, linear section of the tensile test raw data to capture the elastic modulus before the fiberglass tabs started slipping from the coupon. As a result, we could not collect data on the maximum tensile stress of the carbon fiber in our first tensile test. In our second tensile test, we were limited by the demand of the lab by PhD students, so only two specimens were brought to failure for the maximum tensile stress measurement.

Due to the difficulty of attaching the empty weight of the small aircraft to the swinging arm setup, we were only able to test with a drop height of up to 2 inches. Any higher of a height would have resulted in the masses tipping over, posing potential danger if people weren't wearing proper footwear. With more time, our team would investigate superior methods of attaching weights to simulate the weight of the aircraft.

With horizontal and vertical boundary conditions exerted on the bolt hole connecting to the wheels, there is a stress concentration on the edges of the hole. In order to make the FEM more robust, it would be advisable to instead of placing deflection boundary conditions, exert impact loads on the structure. In this experiment, we were limited by time of simulation; a simple model of this

type would take 12-15 hours to run. An area of future work would be to invest additional time to improve the robustness of the FEM and its stress outputs.

7 Conclusion

Based on the results we obtained from our experimentation, the composite landing gear is stronger, lighter, and more flexible than the aluminum landing gear. Thus, the carbon landing gear is more desirable than the aluminum landing gear; it satisfies the desirability criterion. We recommend that M-Fly continue its pursuit of using carbon fiber as an alternative to their conventional aluminum landing gear. We also recommend that they use the finite element analysis model we developed for further investigation into future designs.

8 Cost and Schedule

The project has been completed within the 3 months allotted in a semester. In Figure 15, the gray indicates the estimated time that projects would be completed, while the black represents the actual completion time. While some aspects were started later than expected, it was still possible to complete the project by April 28, 2019.

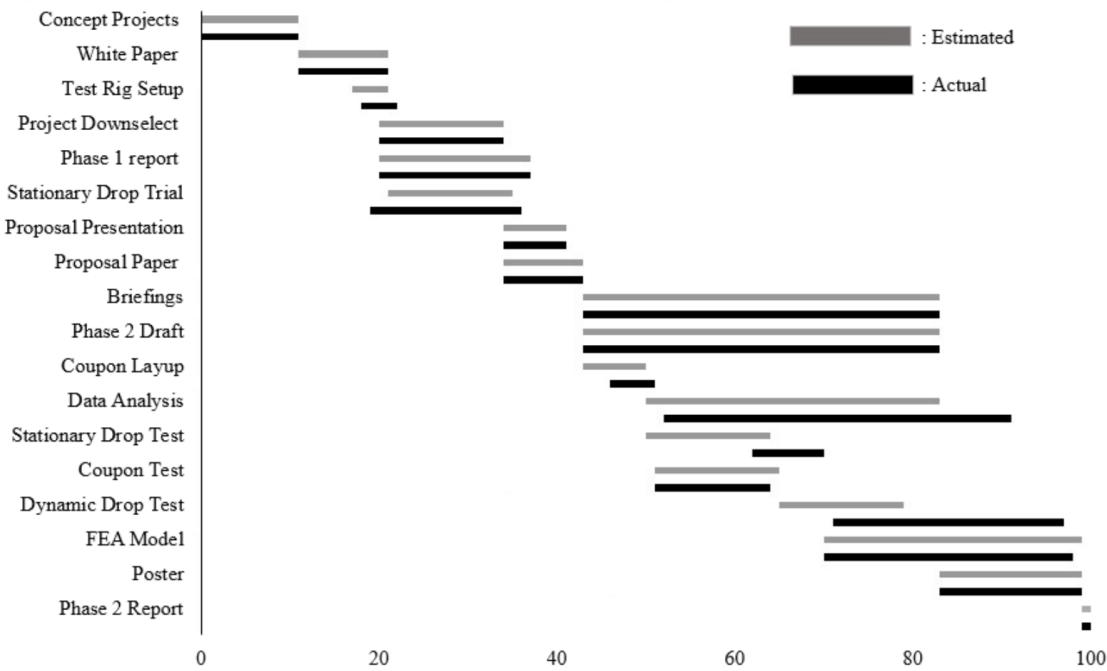


Figure 15: Gantt chart: Work completed within 3 month time period

In addition, the project has been completed for under \$80,000, with \$329.29 spent on supplies, as seen in Tables 6 and 7 and Utilizing the overhead and contingency from the proposed costs, we have completed our project for 385 less than what was estimated, due to less time spent with our consultant than expected and M-Fly providing us with resources for the project.

Table 6: Cost of materials for testing is under \$400 budget

| Material | Unit Cost [\$] | Units | Cost [\$] |
|----------------------|----------------|-------|-----------|
| Accelerometers | 7.95 | 3 | 23.85 |
| Breadboard | 5.95 | 1 | 5.95 |
| Rollers | 26.90 | 4 | 107.60 |
| Strain Gauges | 65.34 | 2 | 130.68 |
| Aluminum Stock | 47.11 | 1 | 47.11 |
| Sliding Nuts | 9.25 | 1 | 9.25 |
| White Lithium Grease | 4.85 | 1 | 4.85 |
| Total | | | 329.29 |

Table 7: Total cost of project is under \$80,000

| Category | Item | Unit Cost | Number of Units | Cost [\$] | Actual Cost [\$] |
|-------------|------------|--------------|-----------------------------|-----------|------------------|
| Labor | Engineer | 40/hr | 5 x 20 hrs/wk x 12 wks | 48000 | 48000 |
| | Consultant | 50/hr | 1 x 1 hr/wk x 12 wks | 600 | 300 |
| Facilities | Shop | 80/hr | 1 shop x 5 days/wk x 12 wks | 4800 | 4800 |
| Materials | | | | 415 | 330 |
| Total | | | | 53815 | 78409 |
| Overhead | | 55% of Total | | 19598 | 0 |
| Contingency | | 10% of Total | | 5381 | 0 |
| Grand Total | | | | 78794 | 78409 |

References

- [1] 5980 Series Universal Testing Systems up to 600 kN (135,000 lbf) Force Capacity
Available:<https://www.instron.us/en-us/products/testing-systems/universal-testing-systems/electromechanical/5900-series/5980-floor-model>
- [2] Aerospace Specification Metals, Inc., "Aluminum 6061-T6; 6061-T651," ASM Material Data Sheet.
Available:<http://asm.matweb.com/search/SpecificMaterial.asp?bassnum=ma6061t6>.
- [3] Al-Mutlaq, S., "Getting Started with Load Cells," *Voltage Dividers*
Available:<https://learn.sparkfun.com/tutorials/getting-started-with-load-cells#resources-and-going-further>.
- [4] ASTM Standard D7264/D7264M—15, 2015, "Standard Test Method for Flexural Properties of Polymer Matrix Composite Materials," ASTM International, West Conshohocken, PA, 2015, DOI: 10.1520/D7264/D7264M-15.
Available:www.astm.org.
- [5] ASTM Standard E111-17, 2017, "Standard Test Method for Young's Modulus, Tangent Modulus, and Chord Modulus," ASTM International, West Conshohocken, PA, 2017, DOI: 10.1520/E0111-04R10
Available:www.astm.org.
- [6] Bruno Guimbal, Airbus (1993). US5224669A. US5224669A.
Available:<https://patents.google.com/patent/US5224669A/en>
- [7] Gibson, Ronald, "Selection of Laminate Designs", *Principals of Composite Material Mechanics*, 4th ed, McGraw-Hill, 1995, pp 257-262
- [8] Howell, William E, Mcgehee, John R., Daugherty, Robert H, and Vogler, William A., "F-106B airplane active control landing gear drop test performance" *NASA technical reports server [online]*, Nov. 1990,
Available:<https://ntrs.nasa.gov/search.jsp?R=19910004132>
- [9] Landing Gear, 23 C.F.R. § 275 (2010).
Available:<https://www.govinfo.gov/content/pkg/CFR-2010-title14-vol1/pdf/CFR-2010-title14-vol1-sec23-725.pdf>.
- [10] Mangalgiri, P D "Composite materials for Aerospace applications", *Bulletin of Materials Science [online]*, Vol. 22, Issue 3, May 1999, pp 657-664,
Available:<https://link.springer.com/article/10.1007/BF02749982>
- [11] McMaster-Carr, "T-Slotted Framing: Roller Wheel for 1-1/2' High Single Rail," *McMaster-Carr*
Available:<https://www.mcmaster.com/47065t63>.
- [12] Ong, C-L and Shen S.B, "The reinforcing effect of composite patch repairs on metallic aircraft structures", *International Journal of Adhesion and Adhesives [online]*, Vol. 12, Issue 1, Jan. 1992, pp 19-26,
Available:<https://www.sciencedirect.com/science/article/pii/014374969290004F>

[13] Subdararaghavan, Veera, "Aero 510: Finite Elements in Mechanical and Structural Analysis 1", Lecture 1, Winter 2019

Appendix

A Figures

A.1 Abaqus Model

In order to provide M-Fly with a comprehensive overview of the loads and deflections expected, the Abaqus simulation was also run for 35 lbs. This is the MTOW of the MX-3 and is representative of the loads that the landing gear can expect while sitting on the runway.

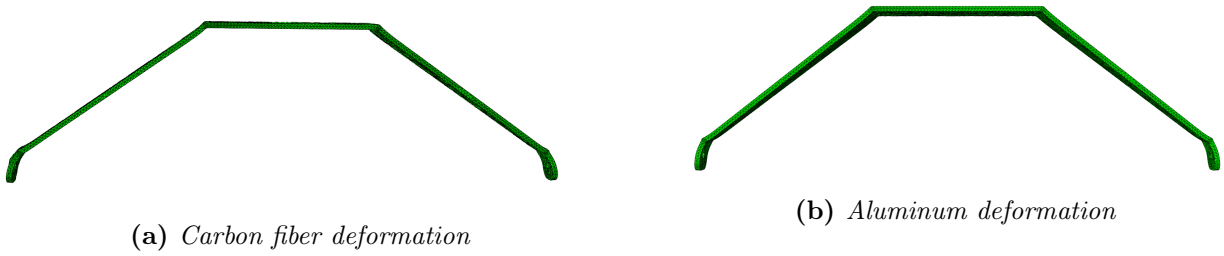


Figure 16: Carbon fiber deforms more than aluminum landing gear at MTOW

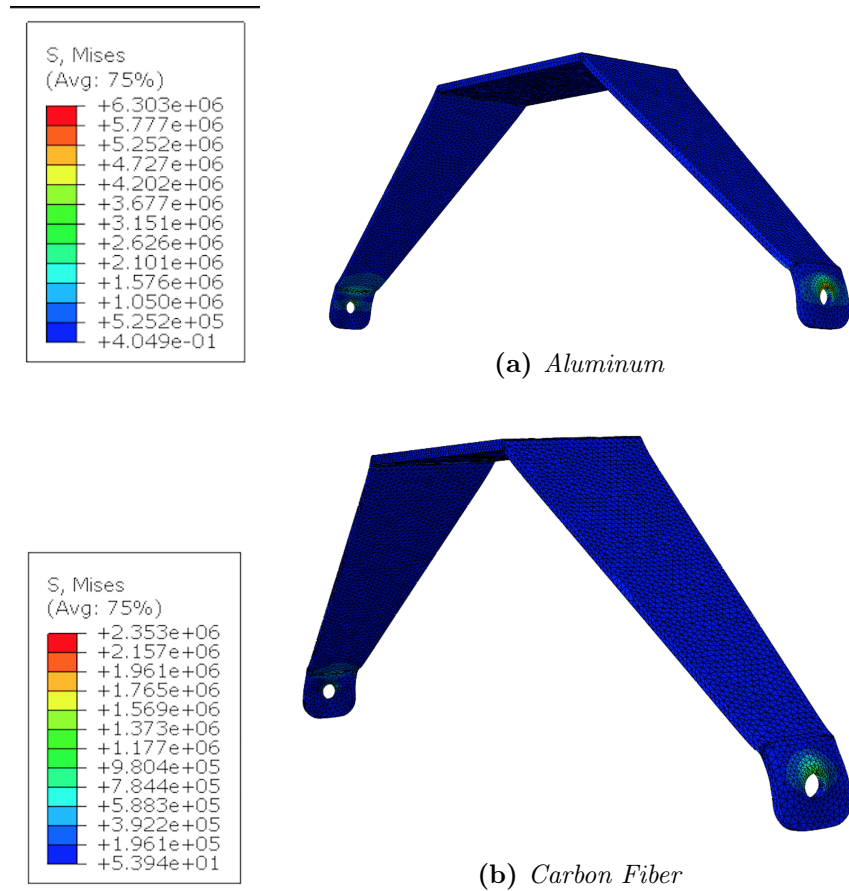


Figure 17: Carbon fiber has lower stresses than aluminum landing gear at MTOW

A.2 Pendulum Test Raw Data

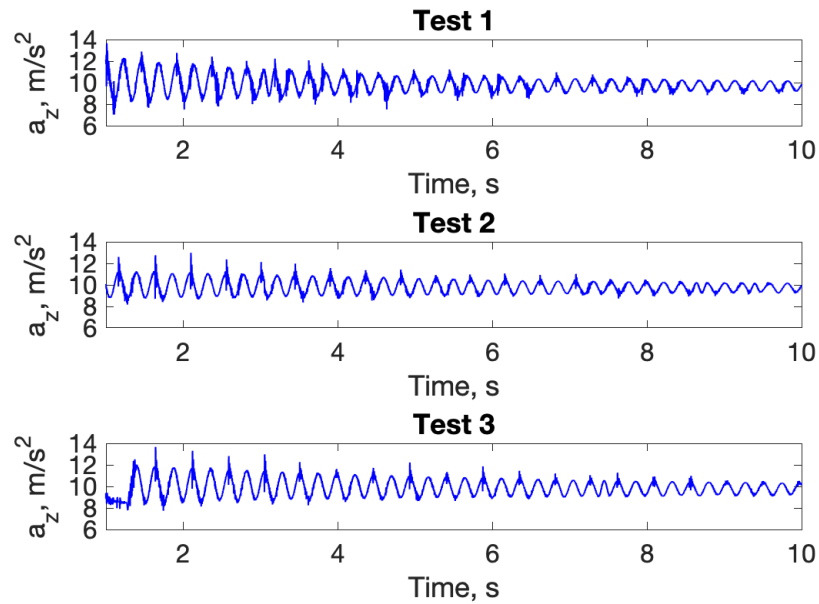


Figure 18: Pendulum test results for setup: $L_1 = 12.75\text{in}$, $\theta = 10^\circ$ follow expected envelope of oscillation

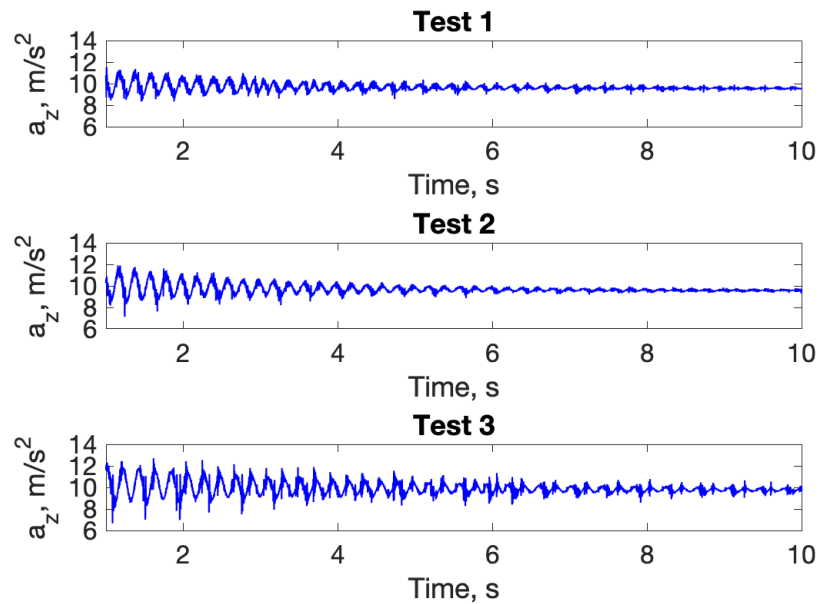


Figure 19: Pendulum test results for setup: $L_2 = 10.25\text{in}$, $\theta = 10^\circ$ follow expected envelope of oscillation

A.3 Tensile Test Raw Data

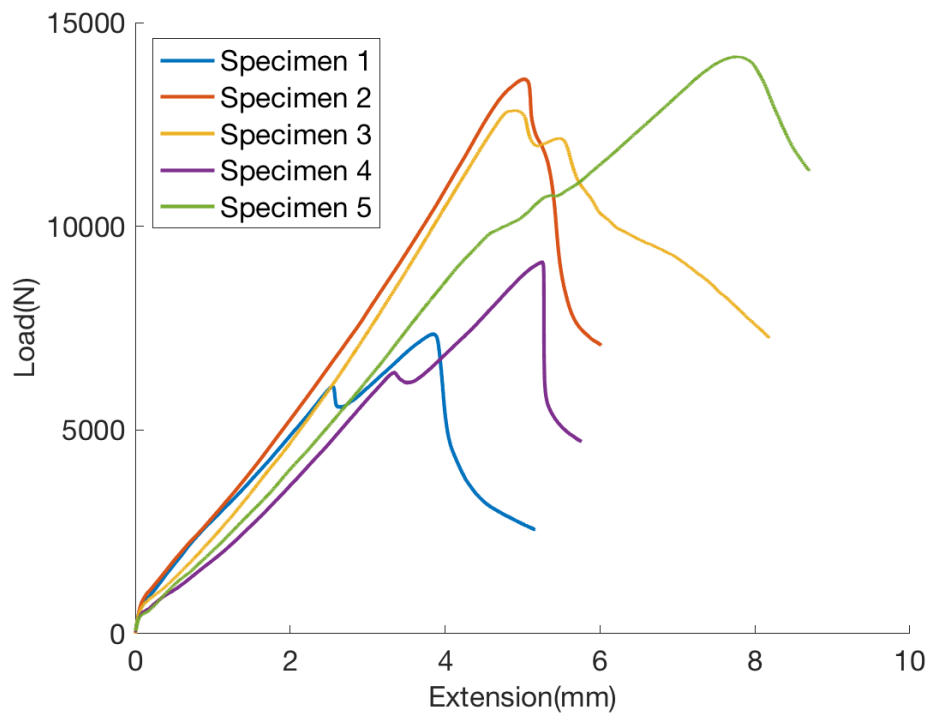


Figure 20: Tensile test raw data shows "bumps" where fiberglass tabs began to slip

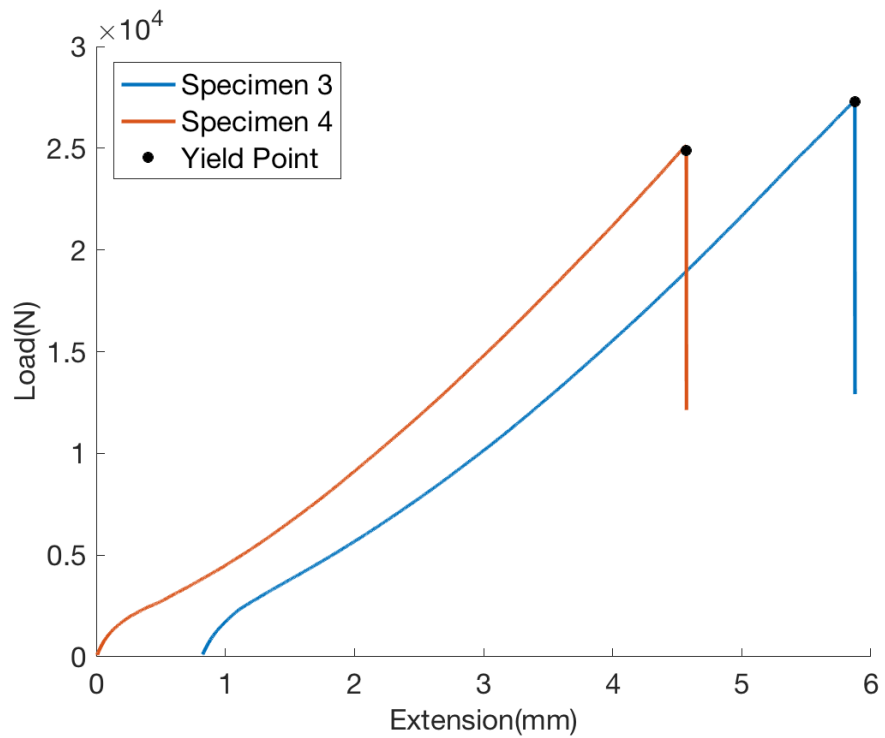


Figure 21: Tensile failure test raw data shows peak load before specimen fracture

A.4 Drop Test Sample Data

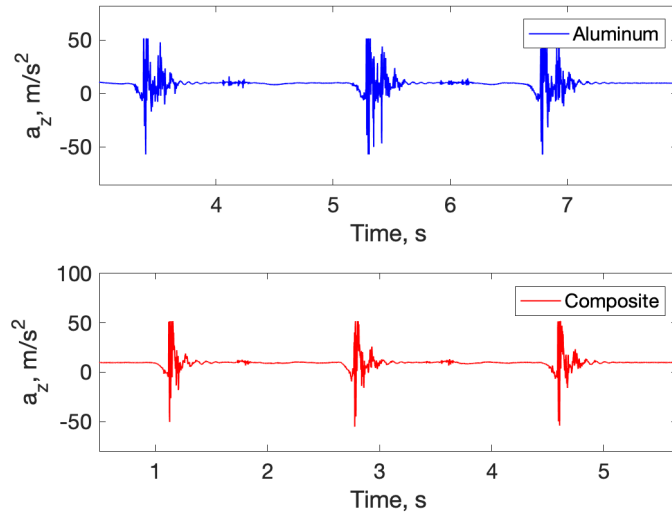


Figure 22: Drop test sample data shows 3 trials of impact duration subsequently used for calculations

B Tables

Table 8: Four-point bending test raw data shows peak load before specimen failure

| Specimen | Max Flexural Stress [MPa] | Flexural modulus of Elasticity [MPa] |
|----------------|---------------------------|--------------------------------------|
| 1 | N/A | 57.02 |
| 2 | 456.81 | 52.99 |
| 3 | 527.09 | 57.71 |
| 4 | 493.45 | 53.52 |
| 5 | 539.59 | 55.35 |
| Average | 504.23 | 55.32 |

Table 9: Results of tensile tests

| Specimen | Elasticity Modulus [GPa] |
|----------------|--------------------------|
| 1 | 30.219 |
| 2 | 29.621 |
| 3 | 32.751 |
| 4 | 26.005 |
| 5 | 27.227 |
| Average | 29.165 |

B.1 Four-Point Bending Test: Specimen Measurements

Table 10: Four-point bending test: specimen measurements

| Specimen | Measurement | Length[in] | Width[in] | Thickness[in] | Data file |
|----------|-------------|------------|-----------|---------------|------------------------|
| 1 | 1 | 5.542 | 0.485 | 0.1285 | Specimen_RawData_1.csv |
| | 2 | 5.5355 | 0.498 | 0.1365 | |
| | 3 | 5.5355 | 0.4945 | 0.145 | |
| 2 | 1 | 5.563 | 0.464 | 0.143 | Specimen_RawData_2.csv |
| | 2 | 5.5535 | 0.419 | 0.136 | |
| | 3 | 5.56 | 0.454 | 0.131 | |
| 3 | 1 | 5.5305 | 0.5065 | 0.1285 | Specimen_RawData_3.csv |
| | 2 | 5.5325 | 0.4935 | 0.1415 | |
| | 3 | 5.529 | 0.51 | 0.148 | |
| 4 | 1 | 5.5465 | 0.492 | 0.1385 | Specimen_RawData_4.csv |
| | 2 | 5.546 | 0.504 | 0.1345 | |
| | 3 | 5.5425 | 0.497 | 0.1315 | |
| 5 | 1 | 5.5335 | 0.513 | 0.1285 | Specimen_RawData_5.csv |
| | 2 | 5.5325 | 0.488 | 0.1405 | |
| | 3 | 5.532 | 0.4795 | 0.1435 | |

B.2 Drop Tests: Impact Times

Table 11: *Drop Test Results for Landing Gear of Two Materials*

| (a) Aluminum Landing Gear | | | (b) Composite Landing Gear | | |
|---------------------------|------------------|-----------------|----------------------------|------------------|-----------------|
| Test | Drop Height (in) | Impact Time (s) | Test | Drop Height (in) | Impact Time (s) |
| 1 | 0.5 | 0.004 | 1 | 0.5 | 0.009 |
| 2 | 0.5 | 0.003 | 2 | 0.5 | 0.008 |
| 3 | 0.5 | 0.003 | 3 | 0.5 | 0.008 |
| 4 | 1.0 | 0.008 | 4 | 1.0 | 0.011 |
| 5 | 1.0 | 0.006 | 5 | 1.0 | 0.013 |
| 6 | 1.0 | 0.010 | 6 | 1.0 | 0.012 |
| 7 | 1.5 | 0.014 | 7 | 1.5 | 0.020 |
| 8 | 1.5 | 0.010 | 8 | 1.5 | 0.013 |
| 9 | 1.5 | 0.011 | 9 | 1.5 | 0.017 |
| 10 | 2.0 | 0.012 | 10 | 2.0 | 0.018 |
| 11 | 2.0 | 0.012 | 11 | 2.0 | 0.021 |
| 12 | 2.0 | 0.013 | 12 | 2.0 | 0.026 |

B.3 Tensile Tests: Specimen Measurements

Table 12: *Tensile tests: specimen measurements*

| Specimen | Length[in] | Width[in] | Thickness | Data file |
|----------|------------|-----------|-----------|--------------------|
| 1 | 5.165 | 0.504 | 0.148 | Specimen_RawData_1 |
| 2 | 5.154 | 0.500 | 0.1425 | Specimen_RawData_2 |
| 3 | 5.1500 | 0.473 | 0.1415 | Specimen_RawData_3 |
| 4 | 5.152 | 0.4995 | 0.1440 | Specimen_RawData_4 |
| 5 | 5.1705 | 0.4905 | 0.1425 | Specimen_RawData_5 |

C Drop Test Derivation

We assume that the mass of the 80/20 beam is m_b , the mass of the landing gear is m_l , the length of the beam (measuring from the tip of the beam to the center of the pivot) is L and the landing gear is dropped from a height of H . From the drop test, we will have z -axis accelerations within a time range $(0, T)$.

According to the conservation of energy, and we assume that the mass distribution of the 80/20 beam is uniform, we have,

$$\Delta P.E. = \Delta K.E. \implies m_l g H + \frac{1}{2} m_b g H = \frac{1}{2} m_l v^2 + \frac{1}{2} I_b \omega^2 \quad (9)$$

where v is the impact velocity of the landing gear, ω is the angular velocity of beam and I is the moment of inertia of the beam. Therefore, we have,

$$I_b = \frac{m_b L^2}{3}, \quad \text{and} \quad \omega = \frac{v}{L}. \quad (10)$$

Together with Equation 9 and 10, we can solve for the impact velocity v analytically,

$$v = \sqrt{\frac{6m_l g H + 3m_b g H}{3m_l + m_b}}. \quad (11)$$

According to the conservation of rotational momentum, and we assume during impact, the force acting on the landing gear is a constant so that the force we calculate is the average impact force \bar{F} .

$$\text{angular momentum change} = I\Delta\omega \implies \bar{F}L\Delta t = \left(\frac{m_b L^2}{3} + m_l L^2\right) Lv, \quad (12)$$

from which we can solve for the average impact force \bar{F} with Equation 11,

$$\bar{F} = \frac{1}{\Delta t} \left(\frac{m_b L^2}{3} + m_l L^2\right) \sqrt{\frac{6m_l g H + 3m_b g H}{3m_l + m_b}}, \quad (13)$$

where Δt is determined from the acceleration readings from the accelerometer.

D Codes

Listing 1: Classical Lamination Theory (CLT) calculation code

```

1 %% AE 405 Classical Lamination Theory (CLT) Calculation
2 %Equations and method from Principles of Composite Material Mechanics by
3 %Ronald F. Gibson
4 %15 plies
5 %12K, 2x2 twill fiber in West Systems epoxy matrix
6 %total thickness = 3.556 mm, ply thickness = 0.14 mm
7
8 %from Soller Aerospace (fabric manufacturer):
9 %Define material properties from the manufacturer.
10 E1 = 33.4*6.894; %0 degree tensile modulus in GPa
11 E2 = 33.4*6.894; %90 degree tensile modulus in GPa
12 v12 = 0.10; %Poisson's ratio
13 G12 = 0.711*6.894; %number taken from Wichita data sheet, bottom plot on
14 %page 124
15
16 %Define angles in ply configuration.
17 theta1 = 0;
18 theta2 = 45;
19 theta3 = 0;
20 theta4 = 45;
21 theta5 = 0;
22 theta6 = 0;
23
24 %Define the order of the angles in the layup.
25 angle = [theta1 theta2 theta3 theta4 theta5 theta6];
26
27 %%CLT
28 %Define Poisson's ratio.
29 v21 = v12*E2/E1;
30
31 %Step 1: Calculate the stiffness matrix, [Q]

```

```

32 |Q = [E1/(1-v12*v21) v12*E2/(1-v12*v21) 0;
33 |    v12*E2/(1-v12*v21) E2/(1-v12*v21) 0;
34 |    0 0 G12];
35
36 %Step 2: Calculate the transformed reduced stiffness matrix, /Qbar]
37 %For +theta (in degrees):
38 for i=1:500
39 %Reduced stiffness matrix elements for ply 1
40 Q11a(i) = Q(1,1)*(cosd(theta1))^4 + Q(2,2)*(sind(theta1))^4 + 2*(Q(1,2)...
41 + 2*Q(3,3))*((sind(theta1))^2)*(cosd(theta1))^2;
42 Q12a(i) = (Q(1,1) + Q(2,2) - 4*Q(3,3))*((cosd(theta1)^2))...
43 *(sind(theta1))^2 + Q(1,2)*((cosd(theta1))^4 + (sind(theta1))^4);
44 Q22a(i) = Q(1,1)*(sind(theta1))^4 + Q(2,2)*(cosd(theta1))^4 + ...
45 2*(Q(1,2) + 2*Q(3,3))*((sind(theta1))^2)*(cosd(theta1))^2;
46 Q16a(i) = (Q(1,1) - Q(1,2) - 2*Q(3,3))*((cosd(theta1))^3)*sind(theta1)...
47 - (Q(2,2) - Q(1,2) - 2*Q(3,3))*((sind(theta1))^3)*cosd(theta1);
48 Q26a(i) = (Q(1,1) - Q(1,2) - 2*Q(3,3))*((sind(theta1))^3)*cosd(theta1)...
49 - (Q(2,2) - Q(1,2) - 2*Q(3,3))*((cosd(theta1))^3)*sind(theta1);
50 Q66a(i) = (Q(1,1) + Q(2,2) - 2*Q(1,2) - 2*Q(3,3))*((cosd(theta1)^2))...
51 *(sind(theta1))^2 + Q(3,3)*((cosd(theta1))^4 + (sind(theta1))^4);
52
53 %Reduced stiffness matrix for ply 1
54 Qba{i} = [Q11a(i) Q12a(i) Q16a(i); ...
55 Q12a(i) Q22a(i) Q26a(i); ...
56 Q16a(i) Q26a(i) Q66a(i)];
57
58 %Reduced stiffness matrix elements for ply 2
59 Q11b(i) = Q(1,1)*(cosd(theta2))^4 + Q(2,2)*(sind(theta2))^4 + 2*(Q(1,2)...
60 + 2*Q(3,3))*((sind(theta2))^2)*(cosd(theta2))^2;
61 Q12b(i) = (Q(1,1) + Q(2,2) - 4*Q(3,3))*((cosd(theta2)^2))...
62 *(sind(theta2))^2 + Q(1,2)*((cosd(theta2))^4 + (sind(theta2))^4);
63 Q22b(i) = Q(1,1)*(sind(theta2))^4 + Q(2,2)*(cosd(theta2))^4 + ...
64 2*(Q(1,2) + 2*Q(3,3))*((sind(theta2))^2)*(cosd(theta2))^2;
65 Q16b(i) = (Q(1,1) - Q(1,2) - 2*Q(3,3))*((cosd(theta2))^3)*sind(theta2)...
66 - (Q(2,2) - Q(1,2) - 2*Q(3,3))*((sind(theta2))^3)*cosd(theta2);
67 Q26b(i) = (Q(1,1) - Q(1,2) - 2*Q(3,3))*((sind(theta2))^3)*cosd(theta2)...
68 - (Q(2,2) - Q(1,2) - 2*Q(3,3))*((cosd(theta2))^3)*sind(theta2);
69 Q66b(i) = (Q(1,1) + Q(2,2) - 2*Q(1,2) - 2*Q(3,3))*((cosd(theta2)^2))...
70 *(sind(theta2))^2 + Q(3,3)*((cosd(theta2))^4 + (sind(theta2))^4);
71
72 %Reduced stiffness matrix for ply 2
73 Qbb{i} = [Q11b(i) Q12b(i) Q16b(i); ...
74 Q12b(i) Q22b(i) Q26b(i); ...
75 Q16b(i) Q26b(i) Q66b(i)];
76
77 %Reduced stiffness matrix elements for ply 3
78 Q11c(i) = Q(1,1)*(cosd(theta3))^4 + Q(2,2)*(sind(theta3))^4 + ...
79 2*(Q(1,2) + 2*Q(3,3))*((sind(theta3))^2)*(cosd(theta3))^2;
80 Q12c(i) = (Q(1,1) + Q(2,2) - 4*Q(3,3))*((cosd(theta3)^2))...
81 *(sind(theta3))^2 + Q(1,2)*((cosd(theta3))^4 + (sind(theta3))^4);
82 Q22c(i) = Q(1,1)*(sind(theta3))^4 + Q(2,2)*(cosd(theta3))^4 + ...
83 2*(Q(1,2) + 2*Q(3,3))*((sind(theta3))^2)*(cosd(theta3))^2;
84 Q16c(i) = (Q(1,1) - Q(1,2) - 2*Q(3,3))*((cosd(theta3))^3)*sind(theta3)...
85 - (Q(2,2) - Q(1,2) - 2*Q(3,3))*((sind(theta3))^3)*cosd(theta3);

```

```

86 | Q26c(i) = (Q(1,1) - Q(1,2) - 2*Q(3,3))*((sind(theta3))^3)*cosd(theta3) ...
87 |   - (Q(2,2) - Q(1,2) - 2*Q(3,3))*((cosd(theta3))^3)*sind(theta3);
88 | Q66c(i) = (Q(1,1) + Q(2,2) - 2*Q(1,2) - 2*Q(3,3))*((cosd(theta3)^2)) ...
89 |   *(sind(theta3))^2 + Q(3,3)*((cosd(theta3))^4) + (sind(theta3))^4);
90 |
91 %Reduced stiffness matrix for ply 3
92 Qbc{i} = [Q11c(i) Q12c(i) Q16c(i);
93   Q12c(i) Q22c(i) Q26c(i);
94   Q16c(i) Q26c(i) Q66c(i)];
95 |
96 %Reduced stiffness matrix elements for ply 4
97 Q11d(i) = Q(1,1)*(cosd(theta4))^4 + Q(2,2)*(sind(theta4))^4 + ...
98   2*(Q(1,2) + 2*Q(3,3))*((sind(theta4))^2)*(cosd(theta4))^2;
99 Q12d(i) = (Q(1,1) + Q(2,2) - 4*Q(3,3))*((cosd(theta4)^2))*...
100   (sind(theta4))^2 + Q(1,2)*((cosd(theta4))^4) + (sind(theta4))^4);
101 Q22d(i) = Q(1,1)*(sind(theta4))^4 + Q(2,2)*(cosd(theta4))^4 + ...
102   2*(Q(1,2) + 2*Q(3,3))*((sind(theta4))^2)*(cosd(theta4))^2;
103 Q16d(i) = (Q(1,1) - Q(1,2) - 2*Q(3,3))*((cosd(theta4))^3)*sind(theta4) ...
104   - (Q(2,2) - Q(1,2) - 2*Q(3,3))*((sind(theta4))^3)*cosd(theta4);
105 Q26d(i) = (Q(1,1) - Q(1,2) - 2*Q(3,3))*((sind(theta4))^3)*cosd(theta4) ...
106   - (Q(2,2) - Q(1,2) - 2*Q(3,3))*((cosd(theta4))^3)*sind(theta4);
107 Q66d(i) = (Q(1,1) + Q(2,2) - 2*Q(1,2) - 2*Q(3,3))*((cosd(theta4)^2)) ...
108   *(sind(theta4))^2 + Q(3,3)*((cosd(theta4))^4) + (sind(theta4))^4);
109 |
110 %Reduced stiffness matrix for ply 4
111 Qbd{i} = [Q11d(i) Q12d(i) Q16d(i);
112   Q12d(i) Q22d(i) Q26d(i);
113   Q16d(i) Q26d(i) Q66d(i)];
114 |
115 %Reduced stiffness matrix elements for ply 5
116 Q11e(i) = Q(1,1)*(cosd(theta5))^4 + Q(2,2)*(sind(theta5))^4 + ...
117   2*(Q(1,2) + 2*Q(3,3))*((sind(theta5))^2)*(cosd(theta5))^2;
118 Q12e(i) = (Q(1,1) + Q(2,2) - 4*Q(3,3))*((cosd(theta5)^2))*...
119   (sind(theta5))^2 + Q(1,2)*((cosd(theta5))^4) + (sind(theta5))^4);
120 Q22e(i) = Q(1,1)*(sind(theta5))^4 + Q(2,2)*(cosd(theta5))^4 + ...
121   2*(Q(1,2) + 2*Q(3,3))*((sind(theta5))^2)*(cosd(theta5))^2;
122 Q16e(i) = (Q(1,1) - Q(1,2) - 2*Q(3,3))*((cosd(theta5))^3)*sind(theta5) ...
123   - (Q(2,2) - Q(1,2) - 2*Q(3,3))*((sind(theta5))^3)*cosd(theta5);
124 Q26e(i) = (Q(1,1) - Q(1,2) - 2*Q(3,3))*((sind(theta5))^3)*cosd(theta5) ...
125   - (Q(2,2) - Q(1,2) - 2*Q(3,3))*((cosd(theta5))^3)*sind(theta5);
126 Q66e(i) = (Q(1,1) + Q(2,2) - 2*Q(1,2) - 2*Q(3,3))*((cosd(theta5)^2)) ...
127   *(sind(theta5))^2 + Q(3,3)*((cosd(theta5))^4) + (sind(theta5))^4);
128 |
129 %Reduced stiffness matrix for ply 5
130 Qbe{i} = [Q11e(i) Q12e(i) Q16e(i);
131   Q12e(i) Q22e(i) Q26e(i);
132   Q16e(i) Q26e(i) Q66e(i)];
133 |
134 %Reduced stiffness matrix elements for ply 6
135 Q11f(i) = Q(1,1)*(cosd(theta6))^4 + Q(2,2)*(sind(theta6))^4 + ...
136   2*(Q(1,2) + 2*Q(3,3))*((sind(theta6))^2)*(cosd(theta6))^2;
137 Q12f(i) = (Q(1,1) + Q(2,2) - 4*Q(3,3))*((cosd(theta6)^2))*...
138   (sind(theta6))^2 + Q(1,2)*((cosd(theta6))^4) + (sind(theta6))^4);
139 Q22f(i) = Q(1,1)*(sind(theta6))^4 + Q(2,2)*(cosd(theta6))^4 + ...

```

```

140 2*(Q(1,2) + 2*Q(3,3))*((sind(theta6))^2)*(cosd(theta6))^2);
141 Q16f(i) = (Q(1,1) - Q(1,2) - 2*Q(3,3))*((cosd(theta6))^3)*sind(theta6) ...
142   - (Q(2,2) - Q(1,2) - 2*Q(3,3))*((sind(theta6))^3)*cosd(theta6);
143 Q26f(i) = (Q(1,1) - Q(1,2) - 2*Q(3,3))*((sind(theta6))^3)*cosd(theta6) ...
144   - (Q(2,2) - Q(1,2) - 2*Q(3,3))*((cosd(theta6))^3)*sind(theta6);
145 Q66f(i) = (Q(1,1) + Q(2,2) - 2*Q(1,2) - 2*Q(3,3))*((cosd(theta6)^2)) ...
146   *(sind(theta6))^2 + Q(3,3)*((cosd(theta6))^4) + (sind(theta6))^4);
147
148 %Reduced stiffness matrix for ply 6
149 Qbf{i} = [Q11f(i) Q12f(i) Q16f(i);
150   Q12f(i) Q22f(i) Q26f(i);
151   Q16f(i) Q26f(i) Q66f(i)];
152
153 %Step 3: Calculate A, B, D matrices that define the stiffness of the
154 %material.
155 %Distances from centerline of laminate:
156 tlam = (3.556e-3)/14; %mm. The 14 is the number of plies, minus 1.
157
158 z0 = -7*tlam; z1 = -6*tlam; z2 = -5*tlam; z3 = -4*tlam; z4 = -3*tlam;
159 z5 = -2*tlam; z6 = -1*tlam; z7 = 0;
160 z14 = 7*tlam; z13 = 6*tlam; z12 = 5*tlam; z11 = 4*tlam; z10 = 3*tlam;
161 z9 = 2*tlam; z8 = 1*tlam;
162
163 %All distances of each ply from the centerline of the thickness:
164 dist = [z0 z1 z2 z3 z4 z5 z6 z7 z8 z9 z10 z11 z12 z13 z14];
165
166 %Define A, B, and D matrices for the composite.
167 Aij = Qba{i}*(z1 - z0) + Qbb{i}*(z2 - z1) + Qbc{i}*(z3 - z2) + Qbd{i}...
168   *(z4 - z3) + Qbe{i}*(z5 - z4) + Qbf{i}*(z6 - z5) + Qbf{i}*(z7 - z6) ...
169   + Qbf{i}*(z8 - z7) + Qbf{i}*(z9 - z8) + Qbe{i}*(z10 - z9) + Qbd{i}...
170   *(z11 - z10) + Qbc{i}*(z12 - z11) + Qbb{i}*(z13 - z12) + Qba{i}*(z14 - z13);
171 Bij = (1/2)*(Qba{i}*(z1^2 - z0^2) + Qbb{i}*(z2^2 - z1^2) + Qbc{i}...
172   *(z3^2 - z2^2) + Qbd{i}*(z4^2 - z3^2) + Qbe{i}*(z5^2 - z4^2) + ...
173   Qbf{i}*(z6^2 - z5^2) + Qbf{i}*(z7^2 - z6^2) + Qbf{i}*(z8^2 - z7^2) ...
174   + Qbf{i}*(z9^2 - z8^2) + Qbe{i}*(z10^2 - z9^2) + Qbd{i}...
175   *(z11^2 - z10^2) + Qbc{i}*(z12^2 - z11^2) + Qbb{i}*(z13^2 - z12^2) ...
176   + Qba{i}*(z14^2 - z13^2));
177 Dij = (1/3)*(Qba{i}*(z1^3 - z0^3) + Qbb{i}*(z2^3 - z1^3) + Qbc{i}*(z3^3 - ...
178   z2^3) + Qbd{i}*(z4^3 - z3^3) + Qbe{i}*(z5^3 - z4^3) + ...
179   Qbf{i}*(z6^3 - z5^3) + Qbf{i}*(z7^3 - z6^3) + Qbf{i}*(z8^3 - z7^3) ...
180   + Qbf{i}*(z9^3 - z8^3) + Qbe{i}*(z10^3 - z9^3) + Qbd{i}...
181   *(z11^3 - z10^3) + Qbc{i}*(z12^3 - z11^3) + Qbb{i}*(z13^3 - z12^3) ...
182   + Qba{i}*(z14^3 - z13^3));
183
184 %Step 4: Put the A, B, and D matrices into the global stiffness matrix, E.
185 Eij = [Aij(1,1) Aij(1,2) Aij(1,3) Bij(1,1) Bij(1,2) Bij(1,3);
186   Aij(2,1) Aij(2,2) Aij(2,3) Bij(2,1) Bij(2,2) Bij(2,3);
187   Aij(3,1) Aij(3,2) Aij(3,3) Bij(3,1) Bij(3,2) Bij(3,3);
188   Bij(1,1) Bij(1,2) Bij(1,3) Dij(1,1) Dij(1,2) Dij(1,3);
189   Bij(2,1) Bij(2,2) Bij(2,3) Dij(2,1) Dij(2,2) Dij(2,3);
190   Bij(3,1) Bij(3,2) Bij(3,3) Dij(3,1) Dij(3,2) Dij(3,3)];
191
192 Eij_inv = inv(Eij);
193

```

```
194 %Step 5: Find the flexural modulus and Young's Modulus
195 Efx = 14/((3.556)^3)*Eij_inv(4,4));
196 Ex = 1/(tlam*14*Eij_inv(1,1));
197
198 end
199
200 %COMMAND WINDOW:
201 %>> Efx
202 %>> Ex
203 %Efx will output the predicted flexural modulus based on Classical
204 %Lamination Theory.
205 %Ex will output the predicted Young's modulus based on Classical
206 %Lamination Theory.
```